Available online at www.sciencedirect.com
ScienceDirect
Journal of Molecular Catalysis A: Chemical 268 (2007) 87–94
JOURNAL OF MOLECULAR CATALYSIS A: CHEMICAL
www.elsevier.com/locate/molcata

Isokinetic behaviour in gas phase catalytic hydrodechlorination of chlorobenzene over supported nickel

Mark A. Keane [a,*], Ragnar Larsson [b]

[a] *Chemical Engineering, School of Engineering and Physical Sciences, Heriot-Watt University, Edinburgh EH14 4AS, Scotland, United Kingdom*
[b] *Chemical Engineering II, University of Lund, PO Box 124, SE 221 00 Lund, Sweden*

Received 20 November 2006; received in revised form 4 December 2006; accepted 5 December 2006
Available online 9 December 2006

Abstract

The kinetics of the hydrodechlorination (HDC) of chlorobenzene has been measured over Ni supported on a range of substrates (MgO, SiO_2, Al_2O_3, Ta_2O_5, MgO, activated carbon (AC) and graphite) of varying BET area (9–843 $m^2\,g^{-1}$) where the Ni loading was in the range 1.5–20.3% (w/w) with catalyst preparation by impregnation and deposition-precipitation. The results of a comprehensive TEM analysis is presented wherein it is demonstrated that the supported Ni phase is present in a range of sizes and morphologies. Compensation behaviour is established for chlorobenzene HDC over these catalysts with an associated isokinetic temperature (T_{iso}) at 669 ± 2 K. Application of the Selective Energy Transfer (SET) model also arrived at the same calculated T_{iso} (669 K). The SET model is based on the premise of resonance between a vibrational mode of the catalyst and a vibrational mode of the reactant with a transferral of resonance energy from the catalyst to the reactant to generate the "activated complex" with subsequent reaction. In this reaction system, resonance results from energy transfer from the catalytic Ni–H vibration (at 940 cm^{-1}) to the out-of-plane C–H vibration (at 740 cm^{-1}) of the reactant. The consequence of lumping together experimental kinetic measurements that show slight variations is discussed and rationalized.

Keywords: Compensation behaviour; Isokinetic temperature; Selective Energy Transfer model; Catalytic hydrodechlorination; Chlorobenzene; Supported Ni catalysts

1. Introduction

In a previous paper [1], we have reported an isokinetic response for the catalytic hydrodehalogenation of a series of halogenated benzene derivatives over a common nickel/silica catalyst. An isokinetic effect arises where the Arrhenius plots ($\ln k$ *versus* $1/T$) for a series of very similar reactions intersect at a common temperature (the isokinetic temperature, T_{iso}). We demonstrated that the T_{iso} for the hydrodehalogenation reactions could be accounted for using the Selective Energy Transfer (SET) model [2]. The basis for the SET model is the occurrence of a state of resonance between a vibrational mode of the catalyst system and a complimentary vibrational mode of the reacting molecule. We identified the critical reactant vibrational mode as an out-of-plane C–H vibration with optimum resonance energy transfer from the catalyst (Ni–H) vibrational mode at 940 cm^{-1} [3]. The T_{iso} predicted from the SET model (655 K) was very close to the value determined experimentally (658 K). In terms of reaction mechanism, we proposed a haloarene/catalyst interaction where the arene molecule is co-planar with the surface and the slow step is an activation of the out-of-plane vibrations of the C–H bond(s).

This result raised the question: will such an agreement also hold for the hydrodehalogenation of a common reactant promoted by a family of catalysts of similar or related composition? Indeed, we can flag a number of studies [4–10] where such a combination has delivered an isokinetic response. We have accordingly, as an extension to our earlier work, taken the hydrodechlorination (HDC) of chlorobenzene as a model reaction promoted by a series of supported Ni catalyts; the raw kinetic data are provided in Table 1. A consensus is emerging from the literature that catalytic hydrodehalogenation is structure sensitive, dependent on metal particle size and electronic structure [11–16]. We consider, in this study, an array of substrates ranging from a basic MgO to conventional Al_2O_3 and SiO_2 as well as Ta_2O_5, a highly refractive oxide

* Corresponding author. Tel.: +44 0131 451 4719
E-mail address: M.A.Keane@hw.ac.uk (M.A. Keane).

1381-1169/$ – see front matter © 2006 Elsevier B.V. All rights reserved.
doi:10.1016/j.molcata.2006.12.007

Table 1
Collation of the experimental chlorobenzene HDC kinetic data

Catalyst	$10^3/T$ (K^{-1})	$\ln(k_{exp}$ mol h^{-1} $g^{-1})$	E_{exp} (kJ mol^{-1})	$\ln A_{exp}$
Ni/SiO_2-I	1.686	−3.252	59.1	8.71
	1.745	−3.669		
	1.808	−4.069		
	1.859	−4.145		
	1.912	−4.876		
	2.008	−5.460		
	2.114	−6.298		
Ni/SiO_2-II	1.686	−3.111	54.7	8.11
	1.745	−3.398		
	1.808	−3.712		
	1.859	−4.056		
	1.912	−4.442		
	2.008	−5.107		
	2.114	−5.894		
Ni/SiO_2-III	1.686	−2.883	51.3	7.58
	1.745	−3.165		
	1.808	−3.589		
	1.859	−3.867		
	1.912	−4.175		
	2.008	−4.834		
	2.114	−5.504		
Ni/SiO_2-IV	1.686	−3.789	63.3	9.22
	1.745	−4.023		
	1.808	−4.482		
	1.859	−4.852		
	1.912	−5.298		
	2.008	−6.078		
	2.114	−6.969		
Ni/SiO_2-V	1.686	−3.806	61.5	8.85
	1.745	−4.078		
	1.808	−4.421		
	1.859	−4.785		
	1.912	−5.224		
	2.008	−5.993		
	2.114	−6.927		
Ni/Al_2O_3	1.686	−3.895	75.5	11.36
	1.745	−4.551		
	1.808	−5.023		
	1.859	−5.612		
	1.912	−5.983		
	2.008	−6.912		
	2.114	−7.809		
Ni/MgO	1.686	−3.545	67.1	10.17
	1.745	−3.945		
	1.808	−4.321		
	1.859	−4.817		
	1.912	−5.184		
	2.008	−6.021		
	2.114	−6.985		
Ni/AC	1.686	−2.887	40.4	5.35
	1.745	−3.066		
	1.808	−3.343		
	1.859	−3.743		
	1.912	−4.025		
	2.008	−4.396		
	2.114	−4.893		
Ni/graphite	1.686	−4.913	119.1	19.20
	1.745	−5.768		
	1.808	−6.856		
	1.859	−7.541		
	1.912	−8.004		
	2.008	−9.546		
	2.114	−11.127		
Ni/Ta_2O_5	1.686	−4.223	99.5	15.91
	1.745	−5.184		
	1.808	−5.712		
	1.859	−6.320		
	1.912	−6.897		
	2.008	−8.021		
	2.114	−9.543		

that exhibits many of the qualities of TiO_2 [17]. The use of graphite, a material known [18] to induce strong metal/support interactions and a high surface area activated carbon (AC) with little or no metal/support interaction have also been investigated.

2. Experimental details

2.1. Catalyst preparation and characterization

Two Ni/SiO_2 catalysts were prepared by impregnation of a Cab-O-Sil 5 M silica (surface area = 194 m^2 g^{-1}) with aqueous solutions of $Ni(NO_3)_2$ to deliver a Ni content of 4.6% (w/w) (denoted Ni/SiO_2-I) and 8.9% (w/w) (denoted Ni/SiO_2-II). Prior to reaction, the catalyst precursors were activated in a 100 cm^3 min^{-1} stream of dry H_2 (99.9%) at a temperature ramp (10 K min^{-1}, controlled using a Eurotherm 91e temperature programmer) to a final temperature of 723 K. The temperature was maintained for 18 h where the catalyst bed temperature was independently monitored using an on-line data logging system (Pico Technology, model TC-08) and found to be constant to within ±1 K. In addition, Ni/SiO_2-II was calcined (10 K min^{-1} in 100 cm^3 min^{-1} stream of air) at 873 K prior to reduction and the activated form is denoted Ni/SiO_2-III. Two further Ni/SiO_2 catalysts were prepared by deposition-precipitation as described elsewhere [19] and activated as above without precalcination: 1.5% (w/w) (denoted Ni/SiO_2-IV) and 20.3% (w/w) (denoted Ni/SiO_2-V). This synthesis route involves the precipitation of a nickel(II) phase onto the silica support by basification of a nickel salt solution/silica suspension *via* the decomposition of urea. Nickel loaded Al_2O_3, Ta_2O_5, and MgO (Sigma–Aldrich) were also prepared by impregnation with aqueous $Ni(NO_3)_2$ and reduced without precalcination. Butanolic $Ni(NO_3)_2$ solutions were used to impregnate activated carbon (G-60, 100 mesh, NORIT) and graphite (synthetic 1–2 μm powder, Sigma–Aldrich) supports. Aqueous solutions were not employed as the carbon support materials are hydrophobic, leading to difficulties with surface wetting that can impact on the ultimate metal dispersion [20]. The Ni content of the catalyst precursors (75–150 μm mesh range) was measured by ICP-OES (Vista-PRO, Varian Inc.) where the analysis was reproducible to within ±2%; Ni content of each sample is given in Table 2. The activated samples were

Table 2
Nickel content, BET area and TEM derived mean Ni particle size ($\bar{d}$) and size range associated with the catalysts considered in this study

Catalyst	% Ni (w/w)	BET area ($m^2\,g^{-1}$)	Ni size range (nm)	$\bar{d}$ (nm)
Ni/SiO_2-I	4.6	179	1–24	11
Ni/SiO_2-II	8.9	176	2–30	16
Ni/SiO_2-III	8.9	173	4–45	21
Ni/SiO_2-IV	1.5	188	1–4	2
Ni/SiO_2-V	20.3	170	1–7	4
Ni/Al_2O_3	8.4	121	1–16	8
Ni/MgO	8.6	102	2–25	15
Ni/AC	8.3	843	2–70	27
Ni/graphite	9.8	9	5–80	29
Ni/Ta_2O_5	7.8	11	2–28	14

passivated at room temperature in a stream of 1% (v/v) O_2/He (mass flow controlled at 20 $cm^3\,min^{-1}$) prior to *ex situ* analysis.

The BET surface areas were measured using the commercial CHEMBET 3000 unit (Quantachrome Instruments), employing a 30% (v/v) N_2/He flow; pure N_2 (99.9%) served as the internal standard. At least 2 cycles of nitrogen adsorption–desorption were employed to determine total surface area using the standard single point method; BET surface area values were reproducible to within ±3% and the values quoted in this paper are the mean. XRD analysis (recorded on a Philips X'Pert instrument using nickel filtered Cu Kα radiation) established that the supported Ni phase exhibits an exclusive cubic symmetry with characteristic peaks at 44.5°, 51.8° and 76.3°, corresponding to (1 1 1), (2 0 0) and (2 2 0) planes. Supported Ni particle size was determined by transmission electron microscopy: JEOL 2000 TEM microscope operated at an accelerating voltage of 200 kV. The catalyst samples were dispersed in 1-butanol by ultrasonic vibration, deposited on a lacey-carbon/Cu grid (300 mesh) and dried at 383 K for 12 h. Selected area electron diffraction (SAED) confirmed that the Ni distributed over each support was present in the metallic form and not as an oxide. At least 650 individual Ni particles were counted for each catalyst and the mean Ni particle sizes are quoted in this paper as the number average diameter ($\bar{d}$):

$$\bar{d} = \frac{\sum_i n_i d_i}{\sum_i n_i} \quad (1)$$

where n_i is the number of particles of diameter d_i.

2.2. Catalysis procedure

Chlorobenzene (Sigma–Aldrich, 99.9%) HDC was conducted with a co-current flow of the chloroarene feed in H_2 under atmospheric pressure in a fixed-bed continuous flow glass reactor over the temperature range 423 K ≤ T ≤ 593 K. Isothermal operation was maintained by diluting the catalyst bed with ground glass (75–150 μm). Interparticle and intraparticle heat transport effects can be disregarded when applying established criteria [21]; the temperature differential between the catalyst particle and bulk fluid phase was <1 K. Plug-flow conditions were operable with reactor diameter/catalyst particle ratio = 90. Mass transport contributions under reaction conditions were evaluated taking the approach outlined previously [22] where the molecular diffusion coefficients were calculated using Satterfield's [23] method. The catalytic system was found to operate with negligible diffusion retardation of the reaction rate; effectiveness factor (η) > 0.99 at 573 K. The catalyst was supported on a glass frit and a layer of glass beads above the catalyst bed served as a heating zone, ensuring that the reactants reached the reaction temperature before contacting the catalyst. A Model 100 (kd Scientific) microprocessor controlled infusion pump was used to deliver the chloroarene feed *via* a glass/PTFE airtight syringe and PTFE line at a fixed (calibrated) rate. The ultra pure (99.999%) H_2 was supplied *via* a Brooks mass flow controller and the flow rate was monitored using a Humonics (Model 520) digital flowmeter. The catalyst weight (W) to inlet molar chloroarene flow rate (F_{Cl}) ratio spanned the range 1–1420 g h mol_{Cl}^{-1} where H_2 was at least 12 times in excess relative to stoichiometric quantities. From a consideration of gas phase reaction equilibrium constants [24,25], HDC under the stated reaction conditions can be taken to be irreversible. Adherence to pseudo-first order kinetics has been demonstrated elsewhere [14,26] and the specific rate constants extracted from a pseudo-first order treatment are given in Table 1. In a series of blank tests, passage of each halogenated feed in a stream of H_2 through the empty reactor, *i.e.* in the absence of catalyst, did not result in any detectable conversion. Product analysis by capillary GC has been described in some detail previously [27]; the detection limit corresponded to a feedstock conversion<0.1 mol%. A halogen (in the form of HCl product) mass balance was performed by passing the effluent gas through an aqueous NaOH (3.5–8.0 × 10^{-3} mol dm^{-3}, kept under constant agitation at ≥300 rpm) trap and monitoring continuously the pH change by means of a Hanna HI Programmable Printing pH Bench-Meter. The concentration of HCl generated was also measured by titrimetric analysis of the NaOH trap solution using a Metrohm (Model 728) Autotitrator ($AgNO_3$, combined Ag electrode); Cl mass balance was complete to better than ±8%. All the data presented here have been generated in the absence of any significant catalyst deactivation where each catalytic run was repeated (up to six times) using different samples from the same batch of catalyst: the measured rates did not deviate by more than ±7%.

3. Results

3.1. Catalyst(s) characteristics

The Ni loading, BET surface area and TEM derived mean Ni particle diameters for the 10 activated catalysts considered in this study are recorded in Table 2; representative TEM images are provided in Fig. 1. The BET areas of the Ni/SiO_2 samples were somewhat lower than that of the SiO_2 support, a response that can be attributed to a partial pore filling, which is more pronounced at higher Ni loadings. Nickel supported on silica exhibited an exclusively pseudo-spherical morphology (see Fig. 1(a)), in keeping with earlier TEM characterization reports [28,29]. Previous studies [19,30] have shown that Ni/SiO_2 prepared by impregnation realizes a relatively weak

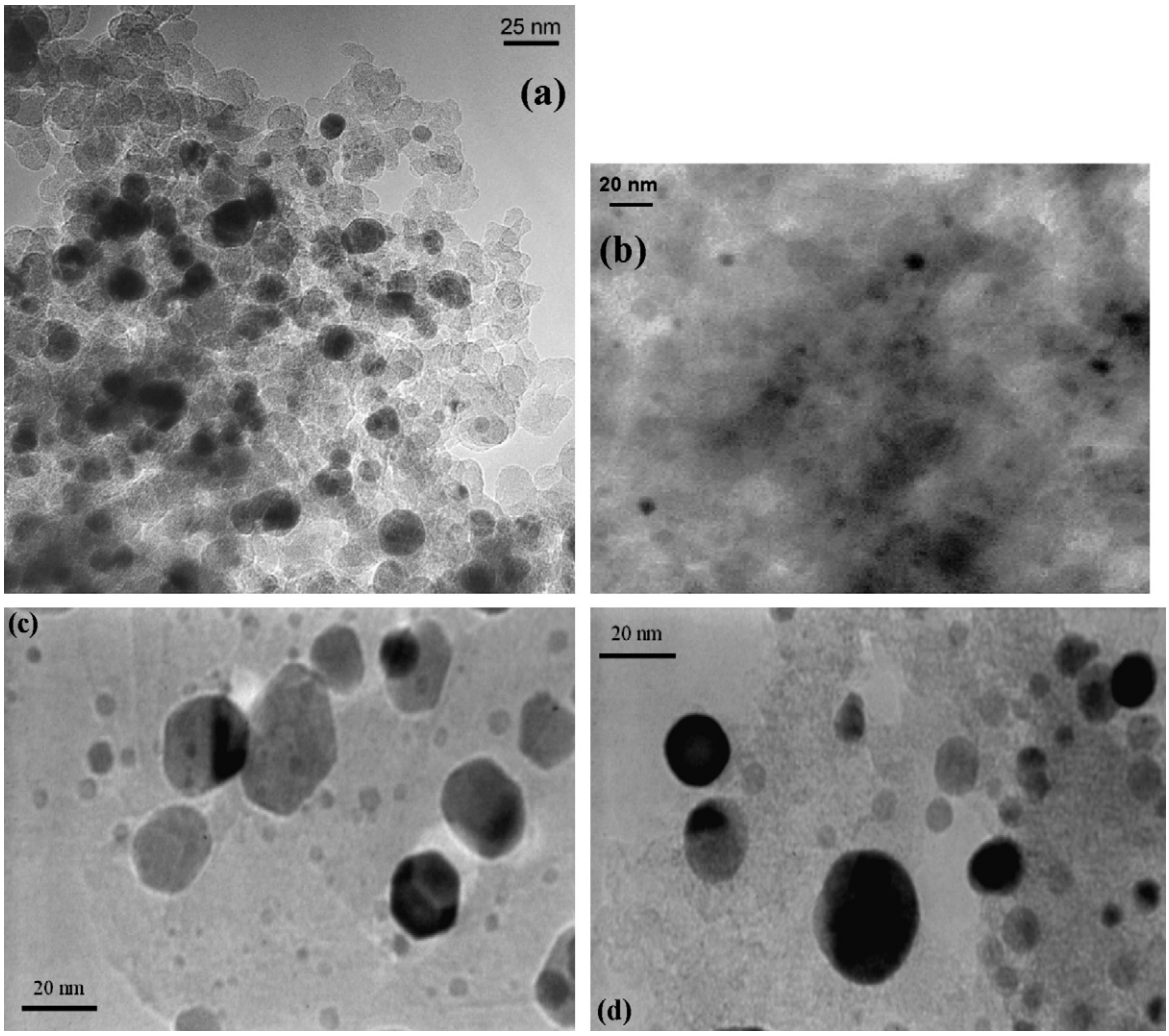

Fig. 1. Representative TEM images of (a) Ni/SiO_2-II, (b) Ni/Al_2O_3, (c) Ni/graphite and (d) Ni/AC.

metal/support interaction resulting in Ni growth during activation, which accounts for the rather wide size distribution (Table 2). An increase in Ni loading (Ni/SiO_2-II *versus* Ni/SiO_2-I and Ni/SiO_2-V *versus* Ni/SiO_2-IV) and the introduction of a calcination step prior to reduction (Ni/SiO_2-III *versus* Ni/SiO_2-II) served to widen the Ni size distribution and increase the mean Ni size as a result of increased particle agglomeration/sintering, as is discussed elsewhere [19,27]. Ni/SiO_2 preparation by deposition-precipitation (Ni/SiO_2-IV and Ni/SiO_2-V) has been shown previously [19,30–32] to generate smaller average Ni particle diameters when compared with the less controlled $Ni(NO_3)_2$ impregnation route. The deposition-precipitation synthesis results in the formation of a nickel phyllosilicate phase that is responsible for enhanced Ni dispersion [33]. Nickel supported on MgO and Ta_2O_5 yielded similar mean Ni size and size distribution to Ni/SiO_2-II which has a comparable Ni loading, albeit the BET surface areas are quite different. The Ni phase associated with Al_2O_3 is characterized by the narrowest Ni particle size distribution and smallest mean Ni size (Table 2) of all the impregnated samples; the nature of the metal dispersion is illustrated in Fig. 1(b). This response finds support in earlier work by Hoang-Van et al. [34]. The suppression of Ni particle growth on alumina has been attributed to the ionic nature of the Ni–Al_2O_3 interaction, leading to an enhanced dispersion of electron-deficient Ni [35]. Graphite has a low (BET) surface area with few edge positions available for depositing the metal that, as a direct consequence, is present in the form of large particles (up to 80 nm, see Table 2), as has been noted elsewhere [36]. Indeed, Ni supported on either carbonaceous (graphite or activated carbon) substrate exhibits a significantly wider size distribution when compared with the oxide supports. Nevertheless, Ni particles on the graphite substrate can be seen in Fig. 1(c) to possess well-defined geometrical shapes, diagnostic of strong metal–support interaction [37]. Reduction of the Ni-impregnated activated carbon (AC), an amorphous substrate with a high BET area, yielded a metal phase of dimensions comparable to that associated with Ni/graphite, albeit a narrower size range and smaller average diameter (Table 2). Growth of Ni particles in this case can be attributed to weaker metal/support interaction, leading to increased Ni mobility and the subsequent greater probability of agglomeration. The weaker Ni–AC interaction is manifested in the spherical/globular nature of the Ni

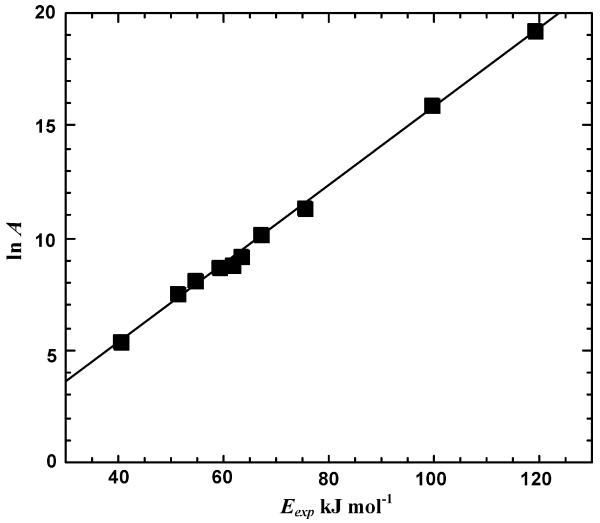

Fig. 2. A "compensation plot" for the HDC of chlorobenzene over the 10 supported Ni catalysts (see Table 2).

particles, as shown in Fig. 1(d). The Ni catalysts considered in this study exhibit some commonality albeit the Ni phase is present in a range of sizes, morphologies and possible electronic perturbations. The remit of this study is to establish some commonality in terms of HDC reaction kinetics and to provide a coherent mechanistic argument to account for this.

3.2. Analysis of experimental HDC data

Chlorobenzene HDC proceeded over each catalyst with 100% selectivity to yield benzene and HCl as the only products; there was no evidence of Cl_2 production or aromatic ring reduction. The raw kinetic data given in Table 1 are presented as a conventional compensation plot, *i.e.* ln *A versus* the experimentally determined activation energy (E_{exp}), in Fig. 2. The linear relationship is consistent with compensation behaviour where the T_{iso} can be extracted from the slope (0.17525 mol kJ^{-1}) according to [7]

$$T_{iso} = \frac{1}{R(\text{slope})} \quad (2)$$

and equals 686 K. This value is close to that (658 K) reported in our earlier paper [1] for the hydrodehalogenation of a family of haloarenes over a common Ni/SiO_2 catalyst. Applying the approach recommended by Linert and Jameson [38], *i.e.* obtaining a T_{iso} from the intersection of the Arrhenius lines associated with the raw experimental data, it can be seen from the entries in Fig. 3 that there is no obvious common point of intersection. However, a closer inspection reveals that the kinetic data generated for the five Ni/SiO_2 catalysts show little variance where the slight differences in activation energy (see Table 1) means that the crossing point cannot be very well defined. We have therefore decided to use a mean value for the Ni/SiO_2 data which is included in Table 3 wherein the equations of the Arrhenius fits (and associated correlation coefficients) are given. A rationale for the use of a mean activation energy is provided later in the text. The Arrhenius plots for the

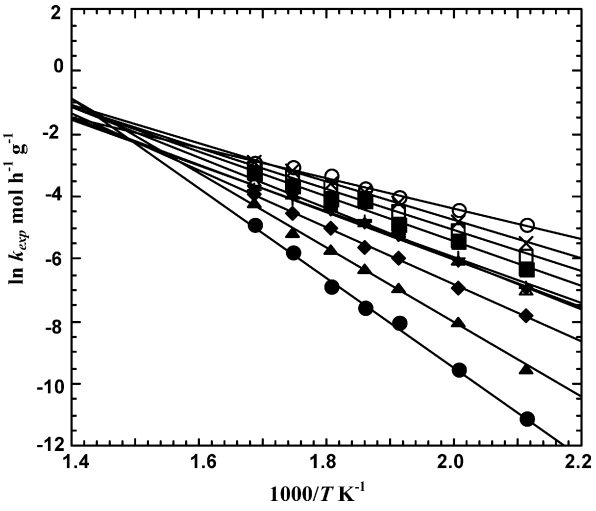

Fig. 3. Arrhenius plots for the HDC of chlorobenzene over all the catalysts studied: (■) Ni/SiO_2-I; (□) Ni/SiO_2-II; (×) Ni/SiO_2-III; (▼) Ni/SiO_2-IV; (+) Ni/SiO_2-V; (♦) Ni/Al_2O_3; (△) Ni/MgO; (◯) Ni/AC; (●) Ni/graphite; (▲) Ni/Ta_2O_3.

Table 3
Formal description of the lines given in Figs. 4 and 5

Catalyst	$y = kx + 1$	R^2 (correlation coefficient)
Ni/SiO_2 (mean)	$y = -6.9805x + 8.5173$	0.99717
Ni/Al_2O_3	$y = -9.0844x + 11.359$	0.99914
Ni/MgO	$y = -8.0708x + 10.167$	0.99783
Ni/AC	$y = -4.8569x + 5.3467$	0.99587
Ni/graphite	$y = -14.325x + 19.125$	0.99862
Ni/Ta_2O_5	$y = -11.959x + 15.934$	0.99781

reduced dataset are shown in Fig. 4 where it can be seen that there is still no perfect point of coalescence. However, a still closer examination allows us to identify two groups of catalysts, *i.e.* Group I (Ni/SiO_2 (mean), Ni/MgO, Ni/AC and Ni/Ta_2O_5) and Group II (Ni/Al_2O_3 and Ni/graphite) that present clear cut examples of an isokinetic relationship, as is illustrated in Fig. 5.

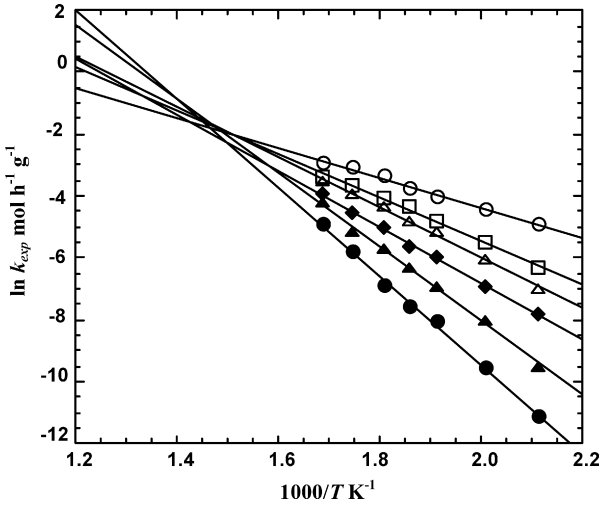

Fig. 4. Arrhenius plots for the HDC of chlorobenzene where the five Ni/SiO_2 catalysts are combined (□) to generate mean values: (♦) Ni/Al_2O_3; (△) Ni/MgO; (◯), Ni/AC; (●), Ni/graphite; (▲) Ni/Ta_2O_3.

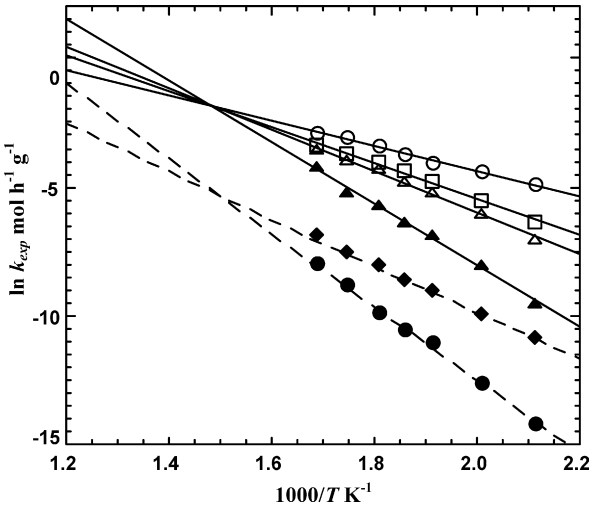

Fig. 5. Arrhenius plots as given in Fig. 4 where the ln k values for Ni/Al_2O_3 (♦) and Ni/graphite (●) have been shifted by a common term to lower values as a visual aid.

It should be noted that the kinetic data for the Group II catalysts has been shifted downwards by 3 units as a visual aid (in Fig. 5) to clearly illustrate the basis for our Group classification. Taking the data for the Group I catalysts plotted in Fig. 5, one can extract a value of $1000/T_{iso} = 1.495 \pm 0.004\ K^{-1}$ which results in a $T_{iso} = 669 \pm 2$ K. The intersection of the two lower lines in Fig. 5 (Group II catalysts) yields $1000/T_{iso} = 1.482\ K^{-1}$, *i.e.* $T_{iso} = 675$ K. Both values of T_{iso} differ slightly from that obtained from the compensation plot in Fig. 2 ($T_{iso} = 686$ K). A $T_{iso} = 669 \pm 2$ K is taken to be a more reliable value to characterize catalytic HDC over supported Ni as it is based on more data than the single point of intersection for the Group II catalysts. Moreover, a higher confidence in the T_{iso} value obtained from the intersection of Arrhenius lines has been established [38] when compared with that which results from the slope of a "compensation line".

3.3. On the origin of the isokinetic temperatures

In our previous paper [1], we demonstrated the pragmatic value of the Selective Energy Transfer (SET) model to account for the isokinetic response exhibited by a group of catalytic hydrodehalogenation reactions. The model is based on the premise that the energy necessary for a reaction to proceed is supplied *via* vibrational resonance; the energy of a vibrator of the catalyst system is transferred to that vibrational mode of the reacting molecule which transforms the molecule towards the "activated state" [2]. From this starting point, where ν represents the wave number of the vibration mode of the reacting molecule and ω is the wave number of the energy source (the catalyst system), it is possible to calculate the isokinetic temperature according to Eq. (3)

$$T_{iso} = NhcR^{-1}(\nu^2 - \omega^2)\omega^{-1} \times \left\{\pm\frac{\pi}{2} - \text{arctg}[0.5\nu\omega(\nu^2 - \omega^2)]^{-1}\right\}^{-1} \quad (3)$$

where N represents the Avogadro number, c the velocity of light, h the Planck constant and R the gas constant. While we have categorized the catalysts into two groups in Fig. 5, the abscissa corresponding to the crossing point for the catalysts in Group I ($1000/T_{iso} = 1.495\ K^{-1}$) is very close to that which characterizes Group II ($1000/T_{iso} = 1.482\ K^{-1}$). Such a slight difference in the isokinetic abscissa for groups of reaction systems is typically accompanied by a corresponding difference in the ordinate position [39]. In order to account for this, we can turn to Eq. (3) which arises from a coupling of the phenomenological expression of the Arrhenius rate law

$$\ln k = \ln Z + \frac{E_{exp}}{R}\left(\frac{1}{T_{iso}} - \frac{1}{T}\right) \quad (4)$$

and the expression derived [2] under conditions of resonance

$$\ln k = \ln Z + \omega(\nu^2 - \omega^2)\omega^{-1}\left(\pm\frac{\pi}{2} - \text{arctg}\frac{\nu\omega}{2(\nu^2 - \omega^2)}\right) \times \sum\frac{\Delta E_i}{hc} - \frac{E_{exp}}{RT} \quad (5)$$

Here Z represents all contributions to the rate constant that are not dependent on SET *via* resonance, *i.e.* "collision number", "form factors", *etc*. It follows that if $T = T_{iso}$, then $\ln k_{iso} = \ln Z$. It is therefore possible for two reaction systems, one with a certain "form factor" and the second system with a "form factor" of (slightly different) magnitude, to generate two different values of $\ln k_{iso}$ but still possess a common value of T_{iso}.

In our previous analysis [1], we assumed that Ni–H vibrations served as the source of catalytic energy, operating on a C–H out-of-plane vibration of the halogenated arene. In this way a transformation from sp^2 to sp^3 hybridization is facilitated, which was deemed necessary for the reaction. From the available literature [3], we chose $\omega = 940\ cm^{-1}$ as the Ni–H vibration (high hydrogen coverage on Raney Ni) that provides the best match to our reaction conditions, *i.e.* hydrogen supply maintained far in excess of reaction stoichiometry where non-competitive adsorption of hydrogen and haloarene prevails [40]. From Eq. (3) we have calculated T_{iso} as a function of the vibrational frequency (ν) of the reacting molecule and the results are presented in Fig. 6. There are four classes of out-of-plane C–H vibrations associated with chlorobenzene [41], which are given in Table 4. In our earlier analysis [1], we adopted the "17b" out-of-plane vibration, *i.e.* $\nu = 902\ cm^{-1}$ which gives (from Eq. (3)) a $T_{iso} = 654$ K that agreed well with the experimentally determined T_{iso} associated with the hydrodehalogenation of 12 different

Table 4
Chlorobenzene C–H out-of-plane vibrations, taken from Varsanyi's compilation [41]

Mode notation	ν (cm^{-1})
5	985
10a	830
10b	196
11	740
17a	965
17b	902

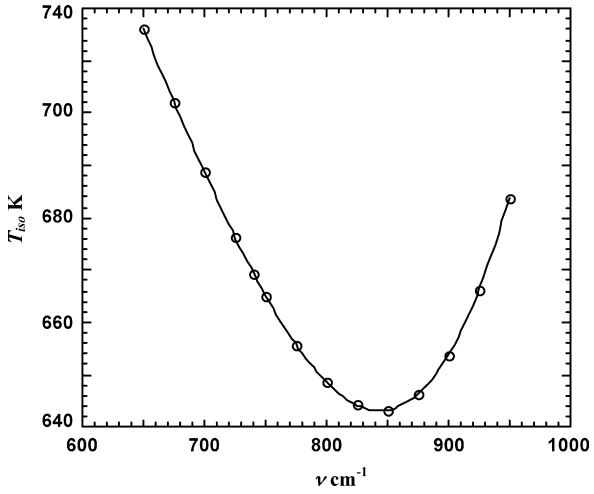

Fig. 6. Calculated (from Eq. (3)) T_{iso} as a function of the frequency of the vibration of the reacting molecule (ν) for an assumed value of the heat bath frequency = 940 cm^{-1}.

haloarene reactants over a common catalyst. However, the T_{iso} generated in this study (669 ± 2 K) is higher than that predicted by adopting the "17b" mode as the critical reactant vibration. Better agreement is reached by applying the vibration mode denoted "11" as that which is excited before reaction. This vibration mode absorbs infrared radiation at 740 cm^{-1} [41] and one can see from the curve presented in Fig. 6 that the associated $T_{iso} \approx 670$ K. Indeed, taking $\omega = 940$ cm^{-1} and $\nu = 740$ cm^{-1}, the calculated (from Eq. (3)) $T_{iso} = 669.2$ K, which represents very good agreement between theory and experiment (T_{iso} = 669 ± 2 K).

The involvement of two different vibrational modes as a composite vibration that "brings the molecule to reaction" is allowed in Eq. (5) where the contribution of one vibrational mode may be greater in terms of overall reaction rate. In our earlier study [1] we demonstrated that, with the exception of polysubstituted haloarenes (with fewer C–H bonds), it was possible to account for the experimentally determined T_{iso} by using the "17b" vibration. The data for all the reactants fell into the range of vibrations that is defined by the curve presented in Fig. 6. The virtue of the "17b" vibration mode is that it exists for even high degrees of benzene substitution [41]. The "11" mode, on the other hand, corresponds to the "umbrella" vibration of benzene (lowest out-of-plane vibrational frequency at 740 cm^{-1}) where all hydrogens (and all carbons) vibrate in-phase. This vibrational mode works well for mono-substituted or *ortho* di-substituted benzenes, where there is still a sufficient number of hydrogens to mimic the umbrella type of motion. In the case of *para* di-substituted species it changes character and disappears [41]. Taking chlorobenzene as reactant, the "11" mode should be effective and our results indicate that it actually supercedes the contribution of the "17b" mode. We must, however, introduce the proviso that we are applying reference values based on free molecule spectral data for chlorobenzene and any catalyst/reactant interaction(s) must result in some deviation of the vibrational frequencies relative to the free molecule. Nevertheless, application of Eq. (3) where $\omega = 940$ cm^{-1} and $\nu = 740$ cm^{-1} generates the isokinetic temperature obtained in this study. The basis for the derivation of Eq. (3) is the classical physics treatment of resonance where the reaction system is treated as a coupled, damped oscillator [2,43]. The question, whether this approach applies for any value of ν has been addressed in an earlier study [44] wherein "good" resonances were taken to be those where the ratio between the two wave numbers could be expressed as the ratio between two small integers. Only in such cases is it acceptable to speak about resonance in a quantum physical sense. We note here that the ratio $\omega/\nu = 1.27$ is very close to 5/4 and the implied interaction between five quanta of ω with four quanta of ν is in good agreement with tests for the proposed condition of resonance [44].

Table 5
Analysis of consecutive differences (ΔE_{exp}) of the experimentally determined activation energies

Catalyst	E_{exp} (kJ mol^{-1})	ΔE_{exp} (kJ mol^{-1})	n_{guess}	n
Ni/SiO_2 (mean)	58.0			
		17.5	2.08	2
Ni/Al_2O_3	75.5			
		8.4	1.00	1
Ni/MgO	67.1			
		26.7	3.18	3
Ni/AC	40.4			
		78.7	9.38	9
Ni/graphite	119.1			
		19.6	2.33	2
Ni/Ta_2O_5	99.5			
		41.5	4.94	5
Sum		192.4		22

$\sum \Delta E_{exp} / \sum n = 8.75$ kJ mol^{-1} = 731 cm^{-1}.

3.4. Treatment of the Ni/SiO_2 data

In order to justify our lumping together of the five kinetic datasets for Ni/SiO_2, a consideration of the experimentally determined activation energies (E_{exp}) is required. These values are included in Table 5 where the consecutive differences between the E_{exp} values (ΔE_{exp}) are identified. It is a corollary to the deduction of Eq. (3) that the activation energies in such a series should change in a stepwise fashion with a least common term that is dependent on the frequency (ν). The basis and application of this "rule" has received a full treatment elsewhere [42,43]. The differences in activation energy (ΔE_{exp}) in such a series can be expressed as a multiple of the least common term [43]. In the first instance, we must guess the least common term; let us take the lowest tabulated value (Table 5), *i.e.* 8.4 kJ mol^{-1}. From this we obtain a "guessed" factor by dividing the differences by 8.4; the resulting number is denoted by n_{guess}. Thereafter we take n_{guess} to the nearest whole number (n) and sum the n values. A more precise value of the common least term is then obtained from

$$\frac{\sum \Delta E_{exp}}{\sum n} \quad (6)$$

and we arrive at a common least term equal to 8.75 kJ mol^{-1}, a value that is greater than any of the differences (from the mean value) of the five Ni/SiO_2 sets. With the corresponding small shifts in the slopes of the Arrhenius lines, no well-defined point of intersection can be expected. These small variations may be attributed to differences in metal/support interaction or metal particle size, while the contribution of experimental error cannot be discounted. The value of the common least term (8.75 kJ mol^{-1}) corresponds to $\nu = 731\ \text{cm}^{-1}$ as

$$E(\text{J mol}^{-1}) = hc\left(\frac{1}{\lambda}\right)N \tag{7}$$

which is in close agreement with the chlorobenzene out-of-plane vibration (740 cm^{-1}) that we take to be involved in the critical activation step. Similar correspondence between the wave numbers arrived at from energy data and spectroscopic values have been reported elsewhere [42,45]. This analysis serves to support our use of a mean E_{exp} for the five Ni/SiO_2 catalysts.

4. Conclusions

Compensation behaviour has been established for the gas phase HDC (where $423\ \text{K} \leq T \leq 593\ \text{K}$) of chlorobenzene over Ni impregnated SiO_2, MgO, Al_2O_3, Ta_2O_5, activated carbon and graphite at a similar Ni loading ($9 \pm 1\%$, w/w). The inclusion of Ni/SiO_2 prepared by deposition-precipitation, the introduction of a precalcination step and variation in Ni loading (1.5–20.3%, w/w Ni) ensured a significant HDC database for a family of related catalysts where comprehensive TEM analysis has demonstrated a range of mean Ni particle sizes, size distributions and morphology. HDC proceeded with 100% selectivity to yield benzene and HCl as the only products where the reaction was conducted in the absence of any significant mass or heat transfer limitations with an overall raw rate measurement reproducibility better than ±7%. Analysis of the experimental results delivers an isokinetic temperature (T_{iso}) at $669 \pm 2\ \text{K}$. The occurrence of this T_{iso} is accounted for in terms of the Selective Energy Transfer (SET) model where an out-of-plane C–H vibration (ν) by chlorobenzene matches a complimentary catalyst vibrational mode (ω) to ensure optimum resonance energy transfer. We have identified the critical chlorobenzene vibration mode as that denoted by "mode 11" in the archival literature (with a characteristic vibration at $\nu = 740\ \text{cm}^{-1}$) where all the ring hydrogens (and carbons) vibrate in-phase. We have established that the catalytically significant vibrational mode ($\omega = 940\ \text{cm}^{-1}$) corresponds to Ni–H surface vibration. The results are consistent with an interaction between five quanta of ν with four quanta of ω that provides the necessary conditions for resonance leading to the activated state. The experimental results for the five Ni/SiO_2 catalysts have been lumped together as a single "mean value", a treatment that we justify on the basis that the successive values of individual E_{exp} differ by less than the common least term.

References

[1] M.A. Keane, R. Larsson, J. Mol. Catal. A: Chem. 249 (2006) 158.
[2] R. Larsson, J. Mol. Catal. 55 (1989) 70.
[3] C.M. Mate, B.E. Bent, G.A. Somorjai, in: Z. Paal, P.G. Menon (Eds.), Hydrogen Effects in Catalysis, Marcel Dekker Inc., New York, 1988, Chapter 2.
[4] D. Lomot, W. Juszczyk, Z. Karpinski, R. Larsson, J. Mol. Catal. A: Chem. 186 (2002) 163.
[5] A. Wootsch, Z. Paál, J. Catal. 205 (2002) 86.
[6] A. Wootsch, Z. Paál, J. Catal. 185 (1999) 192.
[7] G.C. Bond, M.A. Keane, H. Kral, J.A. Lercher, Catal. Rev. Sci. Eng. 42 (2000) 323.
[8] R. Larsson, J. Mascetti, Catal. Lett. 48 (1997) 183.
[9] Z. Karpinski, R. Larsson, J. Catal. 168 (1997) 532.
[10] M.K. Oudenhuijzen, J.A. van Bokhoven, D.C. Koningsberger, J. Catal. 219 (2003) 134.
[11] S.B. Halligudi, B.M. Devassay, A. Ghosh, V. Ravikumar, J. Mol. Catal. A: Chem. 184 (2002) 175.
[12] W. Juszczyk, A. Malinowski, Z. Karpinski, Appl. Catal. A: Gen. 166 (1998) 311.
[13] A.R. Suzdorf, S.V. Morozov, N.N. Anshits, S.I. Tsiganova, A.G. Anshits, Catal. Lett. 29 (1994) 49.
[14] G. Pina, C. Louis, M.A. Keane, Phys. Chem. Chem. Phys. 5 (2003) 1924.
[15] M.A. Keane, C. Park, C. Menini, Catal. Lett. 88 (2003) 89.
[16] L.N. Zanaveskin, V.A. Aver'yanov, Yu.A. Treger, Russ. Chem. Rev. 65 (1996) 617.
[17] S.J. Tauster, S.C. Fung, R.T.K. Baker, J.A. Horsley, Science 211 (1981) 1121.
[18] N.M. Rodriguez, J. Mater. Res. 8 (1993) 3233.
[19] M.A. Keane, Can. J. Chem. 72 (1994) 372.
[20] C. Park, R.T.K. Baker, J. Phys. Chem. B 102 (1998) 5168.
[21] J.R. Welty, C.E. Wicks, R.E. Wilson, Fundamentals of Momentum, Heat and Mass Transfer, John Wiley, New York, 1984.
[22] G. Tavoularis, M.A. Keane, J. Chem. Technol. Biotechnol. 74 (1999) 60.
[23] C.N. Satterfield, Heat Transfer in Heterogeneous Catalysis, M.I.T. Press, Cambridge, MA, 1970.
[24] E.-J. Shin, M.A. Keane, Chem. Eng. Sci. 54 (1999) 1109.
[25] E.-J. Shin, M.A. Keane, J. Chem. Technol. Biotechnol. 75 (2000) 159.
[26] M.A. Keane, Appl. Catal. A: Gen. 271 (2004) 109.
[27] K.V. Murthy, P.M. Patterson, M.A. Keane, J. Mol. Catal. A: Chem. 225 (2005) 149.
[28] C. Park, M.A. Keane, Catal. Commun. 2 (2001) 171.
[29] C. Park, M.A. Keane, J. Catal. 221 (2004) 386.
[30] P. Burattin, M. Che, C. Louis, J. Phys. Chem. B 101 (1997) 7060.
[31] J.W.E. Coenen, Appl. Catal. 75 (1991) 193.
[32] G. Pina, C. Louis, M.A. Keane, Phys. Chem. Chem. Phys. 5 (2003) 1924.
[33] P. Burattin, M. Che, C. Louis, J. Phys. Chem. B 103 (1999) 6171.
[34] C. Hoang-Van, Y. Kachaya, S.J. Teichner, Appl. Catal. 46 (1989) 281.
[35] M.I. Zaki, Stud. Surf. Sci. Catal. 100 (1996) 569.
[36] R.T.K. Baker, E.B. Prestridge, G.B. McVicker, J. Catal. 89 (1984) 422.
[37] R.T.K. Baker, J. Catal. 63 (1980) 523.
[38] W. Linert, R.F. Jameson, Chem. Soc. Rev. 18 (1989) 477.
[39] G.C. Bond, Z. Phys. Chem. 144 (1985) 21.
[40] M.A. Keane, D.Yu. Murzin, Chem. Eng. Sci. 56 (2001) 3185.
[41] G. Varsanyi, Assignments for Vibrational Spectra of Seven Hundred Benzene Derivatives, Adam Hilger, London, 1974.
[42] R. Larsson, Catal. Today 4 (1989) 235.
[43] R. Larsson, React. Kinet. Catal. Lett. 68 (1999) 115.
[44] R. Larsson, M.H. Jamroz, M.A. Borowiak, J. Mol. Catal. A: Chem. 129 (1998) 41.
[45] M. Aresta, A. Dibenedetto, E. Quaranta, M. Boscolo, R. Larsson, J. Mol. Catal. A: Chem. 174 (2001) 7.